THE DYNAMICS OF A SIMPLIFIED PIN-BALL MACHINE

S.R. PRING*AND C.J. BUDD*†

Abstract. In this paper we study the dynamics of an impact oscillator with a modified reset law derived from considering a problem (the pin-ball machine) with an *active impact*. Typical studies of the impact oscillator consider impacts which are governed by Newton's Law of Restitution where the velocity after impact is r times less than the incoming velocity. But in this paper we consider an active impact modelling impacts which occur in a pin-ball machine. In such a machine there exist bumpers which repel the pin-ball at high velocity when an (even slight) impact is made, imparting an additional velocity V to the rebounding pin-ball. Such impacts do not obey the normal laws and in this paper we study how to model them and the subtle dynamics which arises. The analysis proceeds by deriving a one-dimensional map which models the impacts. This map takes the form of a piece-wise linear/square-root map with a discontinuity of size proportional to V. The resulting map is similar in many aspects to a one-dimensional 'map-with-a-gap' but also inherits features of the square-root map. We show how the subtle interplay between these two maps leads to the creation of a very large number of new period orbits, which might explain some of the complexity observed in the dynamics of a true pin-ball machine.

Key words. Non-smooth dynamics, active impact, map with a gap

AMS subject classifications.

1. Introduction. Pin-ball machines are commonly seen in many amusement arcades and are an excellent example of the potential of relatively simple nonlinear mechanical devices to exhibit highly complex dynamics. At the heart of such machines are active 'bumpers' which activate when struck by a pin-ball and (through a simple electro-mechnical/spring mechanism) actively change the momentum of the pin-ball so that it can rebound with a higher relative velocity than it impacts with. We call this device an *active impact system*, in contrast to a *passive impact system* in which the relative rebound velocity is directly proportional to the impact velocity. A significant difference between these two types of problem is that impacts with the bumper at zero velocity (grazing impacts) rebound at a non zero velocity. This has a profound effect on the dynamics which we will explore in this paper.

The dynamics of forced passive impacting systems has been a subject of much study [8] [9] [10] [3] [12] [11] [14] [15] [2] [7] [1] [4] [13] [6], and it is known that it can be very complex, especially when the impacts occur at a low velocity. A simple model of such a passive impact oscillator is given by considering the forced motion of a single-degree-of-freedom particle located at the position $u(t) \geq 0$ which impacts with a fixed obstacle at the position $u = 0$. If $u > 0$ then the particle moves in a free motion and we shall assume that this is governed by the following second-order differential equation

$$\frac{d^2u}{dt^2} + \alpha\frac{du}{dt} + k^2u = f(t), \quad \text{if } u(t) > 0. \tag{1.1}$$

Here α represents the linear damping coefficient of the system and $f(t)$ is a smooth periodic forcing function which we will discuss in more detail later. If $u(t) = 0$ then the particle impacts the obstacle, and we must apply an impact rule. In the case of a

*Centre for Nonlinear Mechanics, Department of Mathematics, University of Bath, UK, BA2 7AY. (S.R.Pring@bath.ac.uk and C.J.Budd@bath.ac.uk)

†Corresponding author

Fig. 1.1: A typical pin-ball machine

passive impacting system it is appropriate to use Newton's Law of Restitution giving

$$\frac{du^+}{dt} = -r\frac{du^-}{dt}, \quad u^+ = u^- = 0 \tag{1.2}$$

where $0 \leq r \leq 1$ is the coefficient of restitution, and du^-/dt and du^+/dt are the velocities of the impact oscillator immediately before and immediately after impact respectively. Even such a simple model has profoundly rich dynamics, with a wide variety of periodic and chaotic forms of motion and unusual transitions (discontinuity-induced-bifurcations) between them. To illustrate some of the dynamics of the passive impact oscillator that can be observed in practice, we present in Figure (1.2) a phase portrait of the asymptotic dynamics of the solution of equations (1.1) and (1.2) with forcing function $f(t) = \cos(\omega(t + t_0)) + d$. In this figure we observe a doubly periodic solution with a single low-velocity impact. As the value of d changes the orbit evolves and at about $d = 0.135$ the impact velocity drops to zero and we observe a *grazing bifurcation* [5]. For $d > 0.135$ we see that a period-1 orbit exists and this represents a non-impacting periodic orbit. As d decreases then a grazing bifurcation occurs at $d = 0.135$ and for $d < 0.135$ we see a period-incrementing cascade of periodic orbits with regions of chaos separating regions of periodic behaviour. A plot of the $\omega-$limit set of the impact oscillator close to the grazing bifurcation is plotted in Figure (1.3) (this bifurcation diagram was computed by sampling the position of the impact oscillator at fixed time intervals equal to the period of the forcing function $f(t)$ taking a large number of random starting configurations). More details, and a classification of the types of behaviour associated with grazing, are given in [5].

In this paper we consider the changes which occur to this type of behaviour in the case of a problem with an active impact. In this case, instead of the coefficient of restitution model alone, we consider an impact which is partly driven by the elastic collision of the particle with the obstacle, and also an impulsive force giving a step change to the momentum. Our motivation for studying such a reset law is that in practise not all impacting systems obey Newton's Law of Restitution and an impacting system which we have in mind is the dynamics which occur in a pin-ball machine. In the center of a pin-ball machine lie circular disks (bumpers) and when the pin-ball strikes one of these disks a switch is turned on which charges a solenoid and in turn

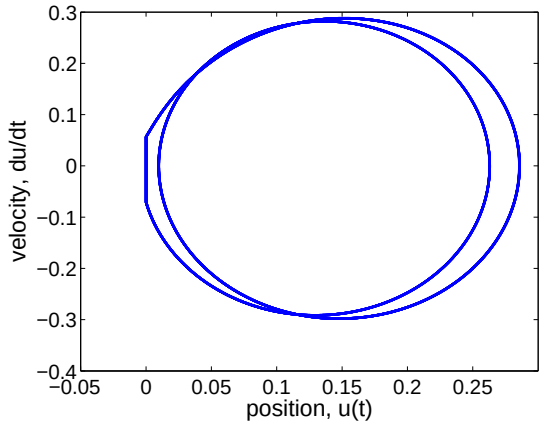

Fig. 1.2: A plot of asymptotic dynamics of the system (1.1) and (1.2) showing a doubly periodic orbit that occurs for parameters $r = 0.8, k = 1, \alpha = 3, \omega = 2.2, t_0 = 0$ and $d = 0.12$.

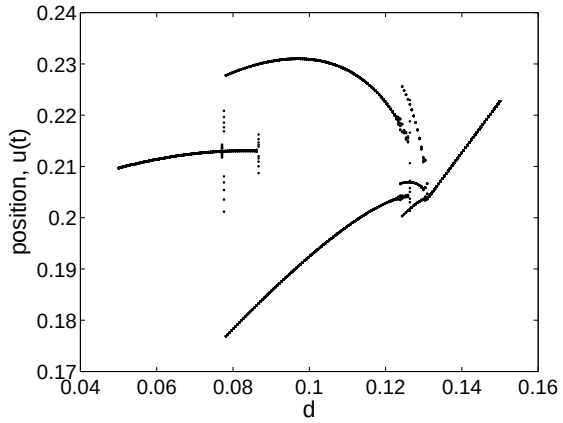

Fig. 1.3: A plot of the bifurcation diagram for the system (1.1) and (1.2) for parameters $r = 0.8, k = 1, \alpha = 3, \omega = 2.2, t_0 = 0$ and varying values of $d = 0.12$.

forces a 'popper ring' to push down on the pinball and mechanically repel the pinball away at high velocity. The interesting dynamics about such an impact is that the pin-ball may leave the impact surface with a higher velocity than it strikes the impact surface. We model the impact dynamics by claiming that the velocity after impact is a combination of both the mechanical impact which is modelled by Newton's Law of Restitution and the momentum change $V > 0$ due to the impulsive force which is imparted on the pin-ball due to the mechanical force which is independent of the incoming velocity. We assume that the velocity after impact is $-rv^- + V$ where $-rv^-$ is due to the normal impact law and V is due to the mechanical force of the popper ring. In this paper we shall typically use a value of $V = 0.4$ and we shall we see that

Fig. 1.4: A picture of a typical pin-ball bumper

the dynamics largely depends on the value of V. Accordingly, we consider an impact law which takes the form

$$\frac{du^+}{dt} = -r\frac{du^-}{dt} + V \text{ at } u(t) = 0 \tag{1.3}$$

where V is a positive constant. One key difference between this system and that of the passive impacting system is that the effect of grazing is more profound, in that an orbit which impacts the obstacle with a very low velocity is changed a great deal from one which only just fails to impact.

We now consider the implications of combining this impact law with the dynamical system described by (1.1). Clearly this is a vast simplification of the true dynamics of a pin-ball machine which has many bumpers and a ball moving in two-dimensions, not to mention the effects of human interaction via the flippers. We approximate the latter action by the use of the periodic forcing as a vast simplification of the action of the human agent in periodically returning the pin-ball to a region close to the bumper. However, the subtle dynamics that we see even in this simple problem gives a hint of the complexity of the dynamics we might expect to see in the true pin-ball machine, and we leave this as a subject for further research.

We now compare the dynamics associated with this law with that of the passive impact which arises in the limit of $V = 0$. To motivate the rest of this paper we plot in Figure (1.5) a phase portrait of a simple periodic orbit of the impact oscillator with reset law (1.3). Again as d is varied we reach a point where the orbit just grazes the obstacle. In Figure (1.6) we plot the resulting bifurcation diagram in the vicinity of this point, again computed again by sampling the position of the impact oscillator periodically.

This bifurcation diagram Figure (1.6) has both similarities to that presented in Figure 1.3. In particular we see a sudden (discontinuous) increase in the size of the attractor after the grazing bifurcation, whereas in Figure (1.3) for the standard impact oscillator there is a continuous square-root growth in the size of the attractor. In this figure we also see further examples of a rich variety of dynamical behaviour. A large number of orbits of high period are created at the grazing bifurcation, with the period of the orbit increasing as the bifurcation point is approached. We also see the phenomenon of *period incrementation* in which a period-n orbit exists in a window Ω_n of the bifurcation parameter, and is replaced (as the parameter approaches the grazing bifurcation point) by a period-$(n+1)$ orbit, with a small interval $\Omega_n \cap \Omega_{n+1}$

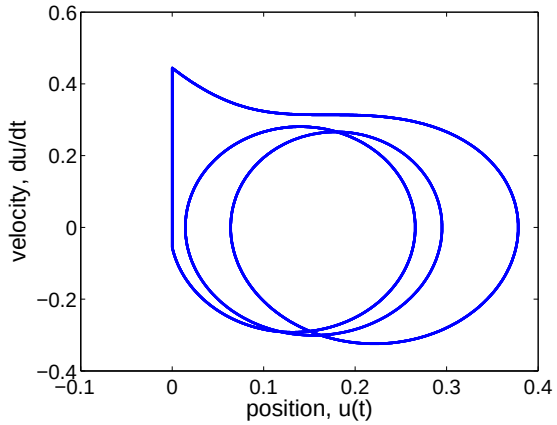

Fig. 1.5: A plot of asymptotic dynamics of the system (1.1) and (1.3) for parameters $r = 0.8, \alpha = 3, k = 1, \omega = 2.2, t_0 = 0, V = 0.4$ and $d = 0.12$.

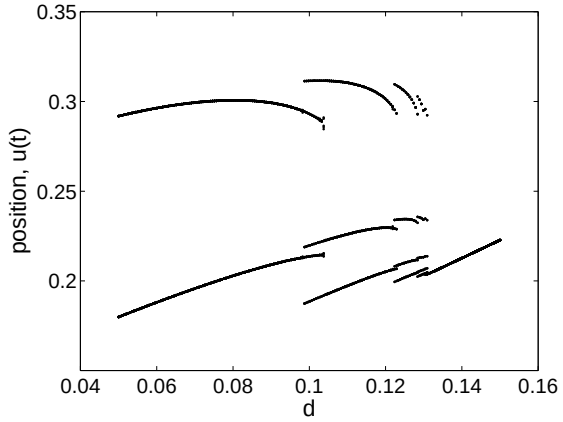

Fig. 1.6: A plot of the bifurcation diagram for the system (1.1) and (1.3) for parameters $r = 0.8, \alpha = 3, \omega = 2.2, t_0 = 0, V = 0.4$ and $d = 0.12$.

where these two orbits co-exist. Significantly such a diagram is very similar in form to the bifurcation diagram associated with a one-dimensional *map with a gap*, see the many references to such in [5]. In this paper we use the zero-time-discontinuity method ZDM described in [5] to derive a two-dimensional Poincaré map of the system (1.1) and (1.3). We then show further that this map reduces to a one-dimensional map using the zero-time discontinuity technique which is outlined in [5] and references therein and a one-dimensional approximation is made to allow a fuller analysis of the problem to be performed. This map takes the form of a piece-wise linear/square-root map with a discontinuity l proportional to the size of the velocity change at the active impact. If $l = 0$ it reduces to the well studied continuous linear/square-root map. However, the introduction of the discontinuity has a profound effect on the

dynamics of this map, the main effect being the creation, and persistence of a very large number of new high period, periodic orbits

The remainder of this paper is organized as follows. In Section 2 a two-dimensional Poincaré map describing both impacting and non-impacting trajectories is derived in the case of an orbit which has a low velocity impact with the active obstacle and a suitable one-dimensional approximation is made by using a suitable change of coordinates. Then in Section 3 an analysis of the behaviour of this map close to a grazing bifurcation is made for suitable parameter values, showing the importance of the active impact parameter l in creating a large number of new periodic orbits.

2. Two-dimensional Poincaré map and one-dimensional approximation. In this Section we use the zero-time discontinuity map (ZDM) to derive a two-dimensional Poincaré map which describes the dynamics of the system (1.1) and (1.3) close to a flow which undergoes a grazing event. We then show how this two-dimensional map can be closely approximated by a one-dimensional map which we analyse in Section 3.

2.1. Derivation of the two-dimensional map close to a grazing event. To derive the (stroboscopic) Poincaré map of this system we sample the position $u(t)$ and velocity $v(t)$ of the impact oscillator at times $t = nT$ where $n \in \mathbb{Z}$ and T equals the period of the forcing function $f(t)$ in equation (1.1). There are two types of Poincaré map which we derive depending on whether or not an impact (or impacts) occurs or not during the sampling time-period $[nT, (n+1)T)$.

To determine the Poincaré map in the absence of impacts, we initially rewrite the periodically forced equation (1.1) in vector form as

$$\dot{\boldsymbol{w}} = B\boldsymbol{w} + \boldsymbol{c}$$

where $\boldsymbol{w}$ is given by

$$\boldsymbol{w} = \begin{pmatrix} u \\ v \end{pmatrix}$$

and matrix B and vector $\boldsymbol{c}$ are defined by

$$B = \begin{pmatrix} 0 & 1 \\ -1 & -\alpha \end{pmatrix} \quad \text{and} \quad \boldsymbol{c} = \begin{pmatrix} 0 \\ f(t;\omega,h,t_0) \end{pmatrix} \equiv \begin{pmatrix} 0 \\ h + \cos(\omega(t+t_0)) \end{pmatrix}.$$

The solution of equation (1.1) (in the absence of any impacts with the obstacle) is given by the identity

$$\boldsymbol{w}(t) = e^{Bt}\boldsymbol{w}(t^*) + \boldsymbol{g}(t)$$

where $\boldsymbol{g}(t)$ is

$$\boldsymbol{g}(t) = e^{Bt}\int_{t^*}^{t^*+t} e^{-B\boldsymbol{s}}\boldsymbol{c}\ d\ \boldsymbol{s}.$$

If we index the position and velocity at time $t = nT$ as u_n and v_n with $\boldsymbol{w}_n$ given as

$$\boldsymbol{w}_n = \begin{pmatrix} u_n \\ v_n \end{pmatrix}$$

then the Poincaré map P_S in general is

$$P_S : \boldsymbol{w}_n \mapsto \boldsymbol{w}_{n+1}.$$

For non-impacting orbits we denote the Poincaré map as P_T. This can be determined directly and is given by:

$$P_T : \boldsymbol{w}_n \mapsto e^{BT}\boldsymbol{w}_n + g(T).$$

Explicitly, the Poincaré map P_T is given by

$$P_T : \begin{pmatrix} u_n \\ v_n \end{pmatrix} \mapsto \begin{pmatrix} a & b \\ c & d \end{pmatrix} \begin{pmatrix} u_n \\ v_n \end{pmatrix} + \begin{pmatrix} g_1 \\ g_2 \end{pmatrix} \tag{2.1}$$

where

$$\begin{pmatrix} a & b \\ c & d \end{pmatrix} = e^{BT} \qquad \text{and} \qquad \begin{pmatrix} g_1 \\ g_2 \end{pmatrix} = e^{BT}\int_0^T e^{-B\boldsymbol{s}}\boldsymbol{c}d\boldsymbol{s}.$$

Of interest to us in the calculation of the dynamics of the pin-ball machine is the comparison of those orbits which just miss the obstacle, with those that impact at a low velocity and, due to the effect of the active impact, then rebound at a much higher velocity. Such orbits will impact the obstacle with a *positive acceleration* $\mathcal{A} > 0$. To derive the map for orbits which impact at low velocity just once during the time interval $[nT, (n+1)T)$ we compose the Poincaré map for a non-impacting orbit P_T with the zero-time discontinuity map which we denote as P_{ZDM}. A full discussion of the zero-time discontinuity mapping technique is given in [5] but we shall derive the zero-time discontinuity map explicitly showing how it works. The zero-time discontinuity map P_{ZDM} is essentially a correction to the Poincaré map for a non-impacting orbit to take into account the fact that an impact has occurred. It can be assumed without loss of generality that if we consider the time interval $[nT, (n+1)T)$ then the impact occurs shortly after time $t = nT$, this assumption can be made rigorous by noting that an arbitrary time constant t_0 exists in the forcing function $f(t) = \cos(\omega(t + t_0)) + d$. To derive the (local) zero-time discontinuity map we denote the position and velocity as $\mathcal{U}$ and $\mathcal{V}$ so as not to confuse with u_n and v_n which are the position and velocity at times $t = nT$. $\mathcal{U}$ and $\mathcal{V}$ are related to u_n and v_n by the relationship $u_n = \mathcal{U}_0$ and $v_n = \mathcal{V}_0$. In Figure (2.1) a sketch is given of the zero-time discontinuity map which is from $(\mathcal{U}_0, \mathcal{V}_0)$ to $(\mathcal{U}_3, \mathcal{V}_3)$.

The map P_{ZDM} can be summarised in the following sequence

$$(\mathcal{U}_0, \mathcal{V}_0) \overset{\delta}{\mapsto} (\mathcal{U}_1, \mathcal{V}_1) \overset{R}{\mapsto} (\mathcal{U}_2, \mathcal{V}_2) \overset{-\delta}{\mapsto} (\mathcal{U}_3, \mathcal{V}_3)$$

where δ denotes a flow forwards of the equation (1.1) by an amount of time δ and R denotes the application of the reset map (1.2). We now compute the terms $(\mathcal{U}_1, \mathcal{V}_1)$, $(\mathcal{U}_2, \mathcal{V}_2)$ and $(\mathcal{U}_3, \mathcal{V}_3)$ in turn.

To compute the ZDM we follow the procedure outlined in [5] and assume that the starting point of the map is such that δ, the time taken for the flow to reach the impact surface from the initial position $(\mathcal{U}_0, \mathcal{V}_0)$, is small and positive. Here we assume that $\mathcal{U}_0$ is small and positive and $\mathcal{V}_0$ is small and negative. Thus, if the initial acceleration is $\mathcal{A}$, the values of $\mathcal{U}_1$ and $\mathcal{V}_1$ are approximately

$$\begin{aligned} \mathcal{U}_1 &= \mathcal{U}_0 + \delta\mathcal{V}_0 + \frac{1}{2}\mathcal{A}\delta^2 + \mathcal{O}(\delta^3) \\ \mathcal{V}_1 &= \mathcal{V}_0 + \delta\mathcal{A} + \mathcal{O}(\delta^2). \end{aligned}$$

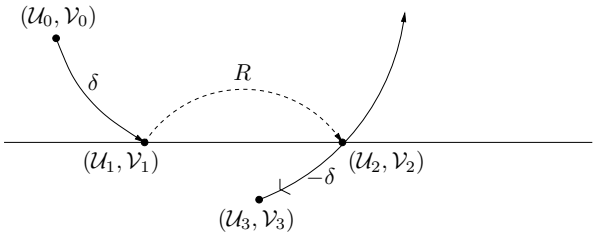

Fig. 2.1: A sketch of the phase-space representation of zero-time discontinuity map $P_{ZDM} : (\mathcal{U}_0, \mathcal{V}_0) \to (\mathcal{U}_3, \mathcal{V}_3)$ for and orbit with positive acceleration $\mathcal{A}$ which impacts the obstacle at a low (negative) velocity. In this figure $\mathcal{U}$ is given by the vertical axis and $\mathcal{V}$ by the horizontal axis. The obstacle is then represented by the horizontal axis.

When the ball reaches the impact surface it rebounds with the additional momentum due to the action of the active impact. This leads to a map (the reset map) R from $(\mathcal{U}_1, \mathcal{V}_1)$ to $(\mathcal{U}_2, \mathcal{V}_2)$. From the conditions of the active impact, we can write this as

$$\begin{array}{rcccl} \mathcal{U}_2 & = & \mathcal{U}_1 & = & \mathcal{U}_0 + \delta\mathcal{V}_0 + \frac{1}{2}\mathcal{A}\delta^2 + \mathcal{O}(\delta^3) \\ \mathcal{V}_2 & = & -r\mathcal{V}_1 + V & = & V - r(\mathcal{V}_0 + \delta\mathcal{A}) + \mathcal{O}(\delta^2). \end{array}$$

To finish this calculation we consider evolving the flow backwards from $(\mathcal{U}_2, \mathcal{V}_2)$ to $(\mathcal{U}_3, \mathcal{V}_3)$ by an amount of time δ. This gives

$$\begin{aligned} \mathcal{U}_3 &= \mathcal{U}_2 - \delta\mathcal{V}_2 + \frac{1}{2}\mathcal{A}\delta^2 + \mathcal{O}(\delta^3) \\ \mathcal{V}_3 &= \mathcal{V}_2 - \delta\mathcal{A} + \mathcal{O}(\delta^2). \end{aligned}$$

Substituting in the expressions for $\mathcal{U}_2$ and $\mathcal{V}_2$ gives

$$\mathcal{U}_3 = (\mathcal{U}_0 + \delta\mathcal{V}_0 + \frac{1}{2}\mathcal{A}\delta^2) - \delta(V - r(\mathcal{V}_0 + \delta\mathcal{A})) + \frac{1}{2}\mathcal{A}\delta^2 + \mathcal{O}(\delta^3) \tag{2.2}$$

$$\mathcal{V}_3 = V - r(\mathcal{V}_0 + \delta\mathcal{A}) - \delta\mathcal{A} + \mathcal{O}(\delta^2). \tag{2.3}$$

To obtain the value of δ at which the impact occurs we must solve the equation $u(\delta) = 0$. A Taylor series expansion of the position gives

$$u(\delta) = \mathcal{U}_0 + \mathcal{V}_0\delta + \frac{1}{2}\mathcal{A}\delta^2 + \mathcal{O}(\delta^3).$$

Setting this to zero and only looking at the smaller of the two solutions, gives the following approximation to δ

$$\delta = \frac{-\mathcal{V}_0 - \sqrt{\mathcal{V}_0^2 - 2\mathcal{A}\mathcal{U}_0}}{\mathcal{A}}.$$

Observe that as $\mathcal{V}_0 < 0$ then $\delta > 0$. Furthermore, impacts only occur if

$$\mathcal{V}_0^2 > 2\mathcal{A}\mathcal{U}_0, \quad \mathcal{V}_0 < 0.$$

Substituting this expression for δ into (2.2) and (2.3) gives

$$\begin{aligned} \mathcal{U}_3 &= \mathcal{U}_0 + \left(\frac{-\mathcal{V}_0 - \sqrt{\mathcal{V}_0^2 - 2\mathcal{A}\mathcal{U}_0}}{\mathcal{A}}\right)((1+r)\mathcal{V}_0 + V) \\ \mathcal{V}_3 &= \mathcal{V}_0 + V + (1+r)\sqrt{\mathcal{V}_0^2 - 2\mathcal{A}\mathcal{U}_0}. \end{aligned}$$

Thus the lowest order expression for the zero-time discontinuity map is

$$P_{ZDM} : \begin{pmatrix} \mathcal{U}_0 \\ \mathcal{V}_0 \end{pmatrix} \mapsto \begin{pmatrix} \mathcal{U}_0 \\ \mathcal{V}_0 + V + (1+r)\sqrt{\mathcal{V}_0^2 - 2\mathcal{A}\mathcal{U}_0} \end{pmatrix}.$$

Equivalently, as $\mathcal{U}_0 \equiv u_n$ and $\mathcal{V}_0 \equiv v_n$ the actual zero-time discontinuity map is given by

$$P_{ZDM} : \begin{pmatrix} u_n \\ v_n \end{pmatrix} \mapsto \begin{pmatrix} u_n \\ v_n + V + (1+r)\sqrt{v_n^2 - 2\mathcal{A}u_n} \end{pmatrix}.$$

To determine the Poincaré map P_S for a single impacting orbit we compose the ZDM with the flow *in the absence of any impacts* so that $P_S = P_T \circ P_{ZDM}$. It follows immediately that P_S is given by

$$\boldsymbol{w}_{n+1} = P_S(\boldsymbol{w}_n) = P_T \circ P_{ZDM}(\boldsymbol{w}_n) = \begin{pmatrix} au_n + b\left(v_n + V + (1+r)\sqrt{v_n^2 - 2\mathcal{A}u_n}\right) + g_1 \\ cu_n + d\left(v_n + V + (1+r)\sqrt{v_n^2 - 2\mathcal{A}u_n}\right) + g_2 \end{pmatrix}. \tag{2.4}$$

For a given set of initial data, we apply this map if an impact occurs, so that $v_n^2 - 2\mathcal{A}u_n \geq 0$. In contrast, if no impact occurs, for $v_n^2 - 2\mathcal{A}u_n < 0$, we simply apply the linear Poincaré map P_T so that

$$\boldsymbol{w}_{n+1} = P_S(\boldsymbol{w}_n) = P_T \circ P_{ZDM}(\boldsymbol{w}_n) = \begin{pmatrix} au_n + bv_n + g_1 \\ cu_n + dv_n + g_2 \end{pmatrix}. \tag{2.5}$$

We observe immediately that this map has a jump discontinuity, caused by the action of the active impact, across the curve $v_n^2 - 2\mathcal{A}u_n \geq 0$. Furthermore, as we approach this curve then we see square-root forms of behaviour. This can be seen clearly in an actual computation. In Figure (2.2) we do this and make a comparison of the analytically derived map and the numerically computed map. In this figure we fix the initial velocity $v(0)$ and vary the initial position $u(0)$. A graze occurs at $u(0) \approx 0.038$ and for $u(0) > 0.038$ there is no impact. For such values of the initial condition, the Poincaré map is linear and we see that there is exact agreement between the two expression for orbits which do not impact. For $u(0) < 0.038$ we have an impact. This leads to the jump discontinuity seen in the figure and the locally square-root behaviour for $u(0)$ less than, and close to, 0.038. The figure demonstrates that the approximate map determined above is in close agreement with the numerical calculations and demonstrates exactly the correct qualitative behaviour both close to, and more distant from, the grazing bifurcation. We now make a one-dimensional approximation which allows a fuller analysis of the bifurcations to be achieved in the next Section.

2.2. The one-dimensional approximation to the impacting Poincaré map. We now determine a one-dimensional approximation of the two-dimensional Poincaré map constructed above. This is achieved by identifying an appropriate non-linear change of coordinates, as outlined in [8] and [7]. To do this we set

$$x_n = v_n^2 - 2\mathcal{A}u_n \qquad \text{and} \qquad y_n = -[dx_n + 2Abv_n + 2\mathcal{A}(dg_1 - bg_2)],$$

so that x_n is the distance from the manifold in phase-space of those initial conditions which lead to an impact. Making a transformation from u_n and v_n into the new coordinate system x_n and y_n, the Poincaré map (2.1) for non-impacting orbits becomes

$$\begin{pmatrix} x_{n+1} \\ y_{n+1} \end{pmatrix} \mapsto \begin{pmatrix} (a+d) & 1 \\ -(ad-bc) & 0 \end{pmatrix} \begin{pmatrix} x_n \\ y_n \end{pmatrix} + \begin{pmatrix} 2\mathcal{A}[(dg_1 - bg_2) - g_1] \\ 0 \end{pmatrix}.$$

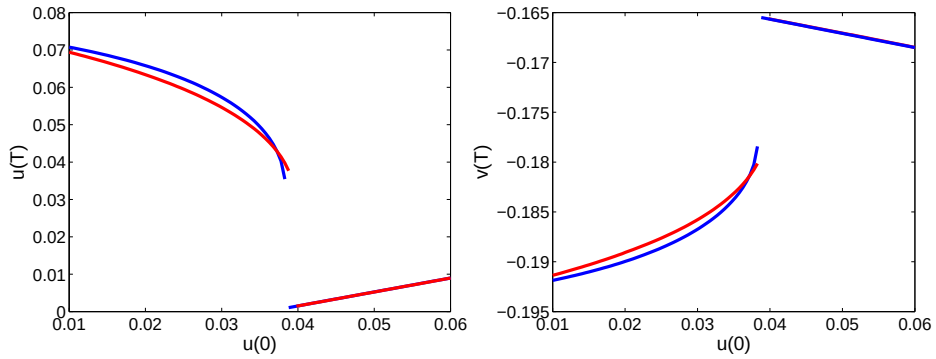

(a) (b)

Fig. 2.2: The red line denotes the analytically derived Poincaré map (2.5) and the blue line denotes the numerical solution for the system (1.1) and (1.3). The map is from $t = 0$ to $t = T = 2\pi/\omega$ with parameters are $\alpha = 3, \omega = 2.1, t_0 = 2.2, r = 0.8, d = 0.11, V = 0.2$ and $0.01 \leq u(0) \leq 0.06$ and initial conditions are $v(0) = -0.23$ for the system (1.1) and (1.3).

Similarly, the Poincaré map (2.5) for impacting orbits becomes

$$\begin{pmatrix} x_{n+1} \\ y_{n+1} \end{pmatrix} \mapsto \begin{pmatrix} (a+d) & 1 \\ -(ad-bc) & 0 \end{pmatrix} \begin{pmatrix} x_n \\ y_n \end{pmatrix} + \begin{pmatrix} -2\mathcal{A}b(1+r)\sqrt{x_n} + 2\mathcal{A}[(dg_1 - bg_2) - g_1] - 2\mathcal{A}bV \\ 0 \end{pmatrix}.$$

In order to obtain a one-dimensional approximation to this map, we follow the analysis presented in [3] and iterate the map producing a significant contraction in the influence of the y coordinate terms. In particular, as

$$ad - bc = \det(e^{BT}) = e^{\text{trace(BT)}} = e^{-\alpha T}$$

then if αT is sufficiently large

$$ad - bc \approx 0.$$

Accordingly the influence of the y contribution in the impacting Poincaré map rapidly becomes negligible, especially if α is not small. We deduce that the two-dimensional map can be approximated by the following one-dimensional map:

$$x_{n+1} = \begin{cases} (a+d)x_n + 2\mathcal{A}[(dg_1 - bg_2) - g_1] & \text{if } x_n < 0 \\ -2\mathcal{A}b(1+r)\sqrt{x_n} + 2\mathcal{A}[(dg_1 - bg_2) - g_1 - bV] & \text{if } x_n \geq 0. \end{cases}$$

We now rescale x_n by introducing a new coordinate $\hat{x}_n$ such that $x_n = (2\mathcal{A}b(1+r))^2\hat{x}_n$ which ensures that the coefficient of the square-root term has magnitude 1. Rescaling x_n and introducing the following parameters

$$\lambda = (a+d), \qquad \mu = \frac{(dg_1 - bg_2) - g_1}{2\mathcal{A}b^2(1+r)^2} \qquad \text{and} \qquad l = \frac{V}{2\mathcal{A}b(1+r)^2}$$

gives the following map

$$x_{n+1} = \begin{cases} \lambda x_n + \mu & \text{if } x_n < 0 \\ -\sqrt{x_n} + \mu - l & \text{if } x_n \geq 0. \end{cases} \tag{2.6}$$

Observe that this map is a combination of the square-root map associated with grazing, with a linear map with a gap that corresponds to the active impact. If $l = 0$ then this is the continuous, piece-wise square-root/linear map that has been widely studied, see [5]. In contrast if $|l|$ is larger than zero then it is closer in form to the piece-wise linear map with a discontinuity. Thus we might expect to see characteristics of both forms of map in the resulting dynamics. We now analyse the dynamics of this map including determining the structure of the bifurcation diagrams and calculating the parameter values at which the map undergoes border-collision and period-doubling bifurcations.

3. Analysis of the one-dimensional map. To begin our analysis, we present a plot of the map (2.6) in Figure (3.1) for parameter values $\lambda = 0.8, l = 1$ and $\mu = 0.5$. For this range of values the map exhibits a stable period-3 orbit, as illustrated. Observe that this periodic orbit has two iterates on the left-hand side of the diagram $x < 0$ in which the linear part of the map is acting, and one iterate on the right-hand side $x > 0$ where the square-root part of the map, with larger stretching, is acting. If we denote any point x_n in an orbit by $\mathcal{L}$ if $x_n < 0$ and $\mathcal{R}$ if $x_n > 0$, then the orbit illustrated has the symbol sequence $\mathcal{LLR}$ or $\mathcal{L}^2\mathcal{R}$. We define a period-N *maximal orbit* to be one with the symbol sequence $\mathcal{L}^{N-1}\mathcal{R}$. Such orbits are the most stable, and the most commonly observed. Such orbits satisfy the conditions

$$x_{n+1} = \lambda x_n + \mu, \quad 1 \le n \le N-1, \quad x_1 = -\sqrt{x_N} + \mu - l, \quad x_1 < x_2 < \ldots < x_{N-1} < 0 < x_N.$$

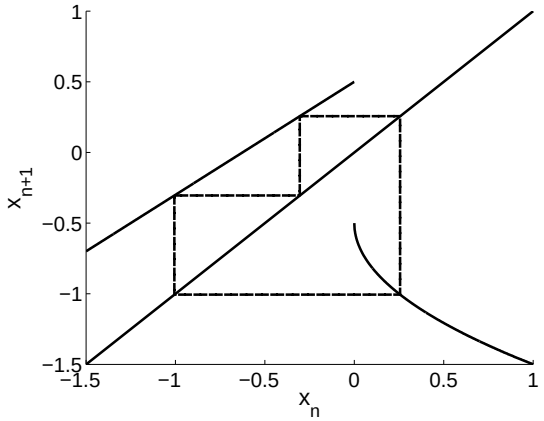

Fig. 3.1: A period-3 orbit of the map (2.6) for parameters $\lambda = 0.8, l = 1$ and $\mu = 0.5$.

To further motivate the analysis of the map (2.6) we plot in Figure (3.2) a bifurcation diagram of the map (2.6) for parameter values which are equivalent to Figure (1.6). In this diagram we give the ω-limit sets of the iterates, which in this case are all maximal periodic orbits with $N - 1$ points $x_j < 0, \quad 1 \le j \le N - 1$ and one point $x_N > 0$. Comparing Figures (3.2) and (1.6) there appears to be good agreement with the qualitative features of both bifurcation diagrams which suggests that our one-dimensional approximate map is a good approximation of the actual dynamics described by the two-dimensional impacting Poincaré map. Indeed, we see a sudden

expansion in the size of the attractor, followed by regions Ω_N in which a period-N (maximal) orbit exists. These intervals intersect for this range of parameters. Indeed what we observe is that $\Omega_N = [\mu_{PD,N}, \mu_{BC,N}]$ where $\mu_{BC,N}$ is a *border-collision* bifurcation point, which occurs when x_{N-1} satisfies the condition $x_{N-1} = 0^-$. In contrast the point $\mu = \mu_{PD,N}$ arises when the period-N maximal orbit loses stability in a *period-doubling bifurcation.*

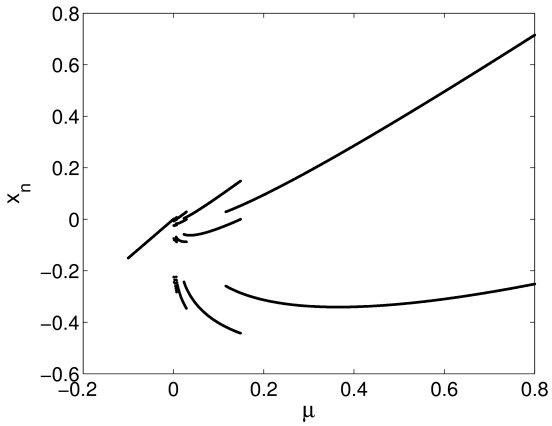

Fig. 3.2: The bifurcation diagram for the map (2.6) with parameters $\lambda = 0.34$ and $l = 0.21$ and these correspond to the physical parameters $\omega = 2.2, r = 0.8, \alpha = 3, V = 0.2, t_0 = 1.4$.

We now determine the existence intervals Ω_N for the period-N maximal orbits of the map (2.6) and examine how these depend upon l and λ.

PROPOSITION 3.1. *The maximal periodic orbits of the form $\mathcal{L}^{N-1}\mathcal{R}$ is stable for $0 < \lambda < 1$ when μ lies in the following interval*

$$\mu \in \Omega_N \equiv [\mu_{PD,N}, \mu_{BC,N}] .$$

Here $\mu_{PD,N}$ denotes the value of μ at which the periodic orbit undergoes a period-doubling bifurcation as μ is decreased and is given as

$$\mu_{PD,N} = \left(\frac{1-\lambda}{1-\lambda^N}\right)\left[\lambda^{N-1} l + \frac{3}{4}\lambda^{2(N-1)}\right].$$

Furthermore, $\mu_{BC,N}$ denotes the value of μ at which the periodic orbit $\mathcal{L}^{N-1}\mathcal{R}$ undergoes a border-collision bifurcation as μ is increased and is given by

$$\mu_{BC,N} = \frac{(1-\lambda)^2}{4(1-\lambda^{N-1})^2}\left[2\lambda^{2(N-2)} + 4l\lambda^{N-2}\left(\frac{1-\lambda^{N-1}}{1-\lambda}\right) + 2\lambda^{N-2}\sqrt{\lambda^{2(N-2)} + 4l\lambda^{N-2}\left(\frac{1-\lambda^{N-1}}{1-\lambda}\right)}\right].$$

Proof. Informally, if we suppose that the periodic orbit $\mathcal{L}^{N-1}\mathcal{R}$ exists and is stable for some fixed value of μ then as μ is increased the single positive iterate x_{N-1}

will tend towards $x = 0$ leading to a border-collision bifurcation when $x_{N-1} = 0$. Conversely, as μ decreases then x_N decreases and the gradient of the map tends to $-\infty$ as $x_N \to 0^+$. Before this, a period-doubling bifurcation occurs when the iterated map has gradient equal to -1.

To substantiate these comments, we let x_N denote the positive iterate, $x_N \geq 0$ so that the value of x_N is given by the condition $f_1^{(N-1)} \circ f_2(x_N) = x_N$ where f_1 and f_2 are given by map (2.6) acting on the sets $x < 0$ and $x > 0$ respectively. By repeated application of the map f_1 and one application of f_2 it is immediate that

$$x_N = \lambda^{N-1} x_1 + \mu \frac{1-\lambda^{N-1}}{1-\lambda}, \quad x_1 = -\sqrt{x_N} + \mu - l.$$

Combining these results, the equation satisfied by x_N is the quadratic equation

$$x_N + \lambda^{N-1}\sqrt{x_N} - \left(\frac{1-\lambda^N}{1-\lambda}\right)\mu + \lambda^{N-1} l = 0.$$

Hence

$$\sqrt{x_N} = \frac{-\lambda^{N-1} + \sqrt{\lambda^{2(N-1)} + 4\left(\left(\frac{1-\lambda^N}{1-\lambda}\right)\mu - \lambda^{N-1} l\right)}}{2}.$$

Note that the positive root term has been taken to ensure $\sqrt{x_N} \geq 0$ consistent with the definition of the map. We see immediately that $\partial x_N / \partial \mu > 0$. The stability of the resulting maximal orbit is determined by the value of $(f_1')^{(N-1)} \circ f_2'(x_N)$ which is given by

$$(f_1')^{(N-1)} \circ f_2'(x_N) = \frac{-\lambda^{N-1}}{2\sqrt{x_N}}.$$

Observe that as μ decreases, then x_N decreases and hence $(f_1')^{(N-1)} \circ f_2'(x_N)$ decreases towards -1. A period-doubling bifurcation occurs when $\mu = \mu_{PD,N}$ at which

$$(f_1')^{(N-1)} \circ f_2'(x_N) = -1$$

and a stable maximal period-N orbit can only be stable if $\mu > \mu_{PD,N}$. Substituting the expression for $\sqrt{x_N}$ the resulting expression for $\mu_{PD,N}$ is then

$$\lambda^{N-1} = -\lambda^{N-1} + \sqrt{\lambda^{2(N-1)} + 4\left(\left(\frac{1-\lambda^N}{1-\lambda}\right)\mu_{PD,N} - \lambda^{N-1} l\right)}.$$

Rearranging once gives

$$\frac{3}{4}\lambda^{2(N-1)} = \left(\frac{1-\lambda^N}{1-\lambda}\right)\mu_{PD,N} - \lambda^{N-1} l$$

and thus $\mu_{PD,N}$ is

$$\mu_{PD,N} = \left(\frac{1-\lambda}{1-\lambda^N}\right)\left[\lambda^{N-1} l + \frac{3}{4}\lambda^{2(N-1)}\right].$$

We now derive the value of μ at which the orbit $\mathcal{L}^{N-1}\mathcal{R}$ undergoes a border-collision as μ is increased. This occurs when the greatest negative iterate, x_{N-1} of the orbit $\mathcal{L}^{N-1}\mathcal{R}$ passes through $x = 0$. The equation for x_{N-1} is $f_1^{(N-2)} \circ f_2 \circ f_1(x_{N-1}) = x_{N-1}$ which explicitly is

$$-\lambda^{N-2}\sqrt{\lambda x_{N-1} + \mu} + \lambda^{N-2}(\mu - l) + \left(\frac{1-\lambda^{N-2}}{1-\lambda}\right)\mu - x_{N-1} = 0.$$

Setting $x_{N-1} = 0$, to give the condition for a border-collision bifurcation then the equation for $\mu_{BC,N}$ is

$$0 = -\lambda^{N-2}\sqrt{\mu_{BC,N}} + (\mu - l)\lambda^{N-2} + \left(\frac{1-\lambda^{N-2}}{1-\lambda}\right)\mu_{BC,N}.$$

Rearranging this leads to a quadratic equation in $\sqrt{\mu_{BC,N}}$ which gives

$$\left(\frac{1-\lambda^{N-1}}{1-\lambda}\right)\mu_{BC,N} - \lambda^{N-2}\sqrt{\mu_{BC,N}} - l\lambda^{N-2} = 0$$

which gives $\sqrt{\mu_{BC,N}}$ as

$$\sqrt{\mu_{BC,N}} = \frac{(1-\lambda)}{2(1-\lambda^{N-1})}\left(\lambda^{N-2} + \sqrt{\lambda^{2(N-2)} + 4l\lambda^{N-2}\left(\frac{1-\lambda^{N-1}}{1-\lambda}\right)}\right).$$

Therefore $\mu_{BC,N}$ is given by

$$\mu_{BC,N} = \frac{(1-\lambda)^2}{4(1-\lambda^{N-1})^2}\left[2\lambda^{2(N-2)} + 4l\lambda^{N-2}\left(\frac{1-\lambda^{N-1}}{1-\lambda}\right) + 2\lambda^{N-2}\sqrt{\lambda^{2(N-2)} + 4l\lambda^{N-2}\left(\frac{1-\lambda^{N-1}}{1-\lambda}\right)}\right].$$

□

NOTE: It is immediate from the conclusions of the Proposition that

$$\mu_{PD,N+1} < \mu_{PD,N} \quad \text{and} \quad \mu_{BC,N+1} < \mu_{BC,N}.$$

A period-N maximal orbit exists provided that $\mu_{PD,N} < \mu_{BC,N}$.

We see from this Proposition that the width and location of the regions of existence Ω_N of the stable maximal period-N orbits depends significantly on the value of l which is proportional to the value of V in the active impact. The case of $l = 0$ corresponds to the continuous piece-wise linear/square-root map and this problem has been studied in great detail [5]. It is known that if $\lambda > 2/3$ then the bifurcation diagram of the $\omega-$limit sets of the map as a function of the parameter μ has a simple period-1 orbit for $\mu < 0$ and a continuous jump to *robust chaos* if $\mu > 0$. If $1/4 < \lambda < 2/3$ then instead of robust chaos we see a period-adding sequence for $\mu > 0$ so that as $\mu \to 0^+$ there exists a series of disjoint windows of existence, Ω_N, of period-N maximal orbits so that $N \to \infty$ as $\mu \to 0^+$. These windows do not intersect, and are separated by intervals in which we observe robust chaos. If $\lambda < 1/4$ then the windows Ω_N intersect.

As we increase l from zero then this picture changes significantly. Firstly we note that the attractor or trapping region for the map (2.6) is the interval

$$[-\sqrt{\mu}+\mu-l,\mu]$$

for $\mu \geq 0$. For $\mu < 0$ a single fixed point exists and at $\mu = 0$ there is a sudden jump from this fixed point to an attractor which is the interval $[-l, 0]$. Furthermore, the width of Ω_N increases in general, leading to regions of intersection which do not occur if $l = 0$. To see these effects, we plot in Figure (3.3) three different bifurcation diagrams of the map (2.6) for $l = 0, 0.1$ and $l = 0.5$ for $\lambda = 0.5$. We can see clearly

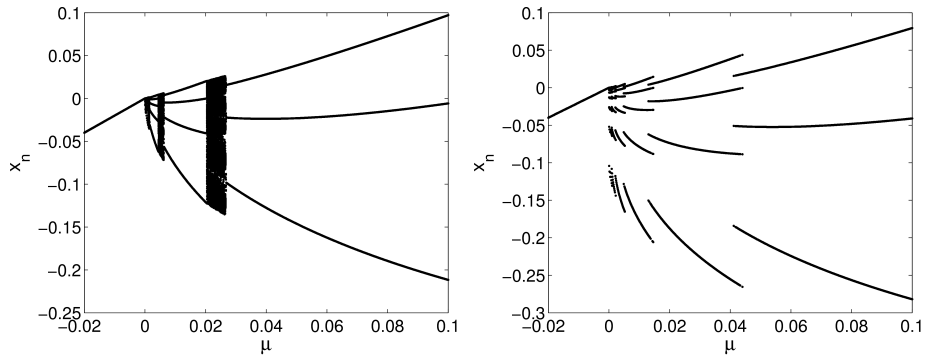

(a) $l = 0$ (b) $l = 0.1$

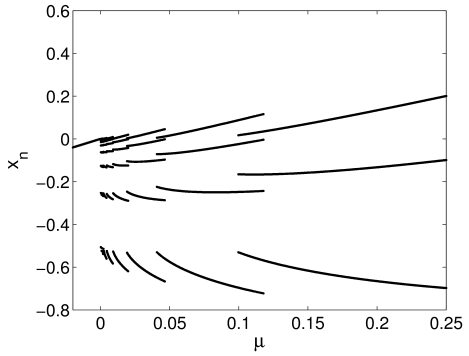

(c) $l = 0.5$

Fig. 3.3: The bifurcation diagrams for the map (2.6) with $\lambda = 0.5$ and the value of l taking the values $l = \{0, 0.1, 0.5\}$.

in these figures that as l increases then the widths of the existence intervals for the periodic orbits increase. For example, for $l = 0$ there is a region of chaos which separates the period-3 and period-4 orbits but for $l = 0.1$ the period-3 and period-4 orbits co-exist and this region of coexistence increases as l increases further to $l = 0.5$. As described above, the size of the jump in the attractor is also dependent on l and this can be clearly seen in Figure (3.3).

To further understand the dynamics and to see explicitly how the width of the existence intervals Ω_N vary, we plot in Figure (3.4) the values of $\mu_{BC,3}$, $\mu_{PD,3}$ and $\mu_{BC,4}$,

$\mu_{PD,4}$ as functions of the parameter l for $\lambda = 0.5$. These values define the existence intervals for the maximal perodic orbits $\mathcal{L}^2\mathcal{R}$ and $\mathcal{L}^3\mathcal{R}$ respectively. Note that if $l = 0$ then these intervals do not intersect if $l = 0$. In contrast, in this figure we can see

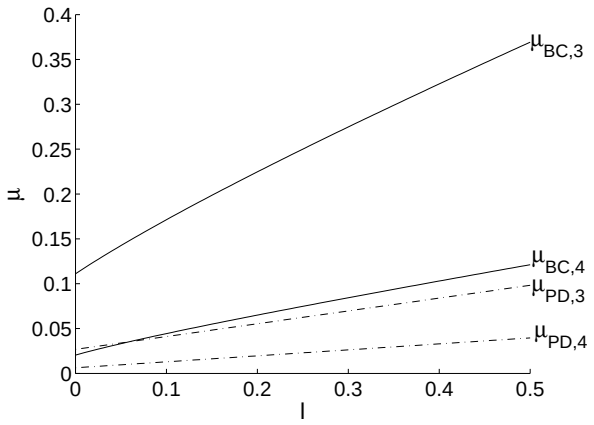

Fig. 3.4: A plot of the period-doubling bifurcation values $\mu_{PD,N}$ denoted by the dashed line and the border-collision values $\mu_{BC,N}$ for $N = 3, 4$ and $\lambda = 0.5$. A periodic orbit exists if $\mu_{PD,N} < \mu_{BC,N}$.

that as l increases then at $l \approx 0.05$ the period-3 and period-4 orbits start to coexist. We note that as l increases further the gap between lines $\mu_{BC,4}$ and $\mu_{BC,3}$ increases. This confirms our earlier observations that the size of the interval $\Omega_2 \cap \Omega_3$ increases with l.

As a second calculation, we plot in Figure (3.5) three different bifurcation diagrams for $l = 0, 0.4, 0.8$ now taking $\lambda = 0.9$. If $l = 0$ then this leads to a region of robust chaos with no stable periodic orbits over an open interval of values of $\mu > 0$, with the first periodic orbit, a period-3 maximal orbit, arising when $\mu \approx 0.17$. However, as l increases away from zero this picture changes. Firstly, it is apparent from these figures that stable high N period-N maximal orbits appear to exist for all values of $\mu > 0$ sufficiently close to $\mu = 0$. For small values of μ these appear to separated by intervals of chaotic behaviour and for larger values of μ the existence intervals of the period-$(N + 1)$ and period-N orbits overlap. As l increases the regions of chaos separating the orbits appear to decrease in width and eventually, the periodic orbits co-exist. This can be seen to occur for the period-3 and period-4 orbit. There is also, as described earlier, a sudden jump in the size of the attractor.

To understand this behaviour further, we plot in Figure (3) the values of

$$\mu_{BC,5} < \mu_{BC,4} < \mu_{BC,3} \quad \text{and} \quad \mu_{PD,5} < \mu_{PD,4} < \mu_{PD,3}$$

as functions of l. In this figure we see that if $l = 0$ then $0.17 \approx \mu_{PD,3} < \mu_{BC,3} \approx 0.22$ indicating (as observed above) that a period-3 orbit exists for values of $\mu > 0.17$. However $\mu_{PD,4} > \mu_{BC,4}$ and $\mu_{PD,5} > \mu_{BC,5}$ indicating that neither the period-4 or the period-5 orbit exists. This result is consistent with the existence of the interval of robust chaos when $l = 0$. As l increases then the curves $\mu_{PD,4}$ and $\mu_{BC,4}$ cross,

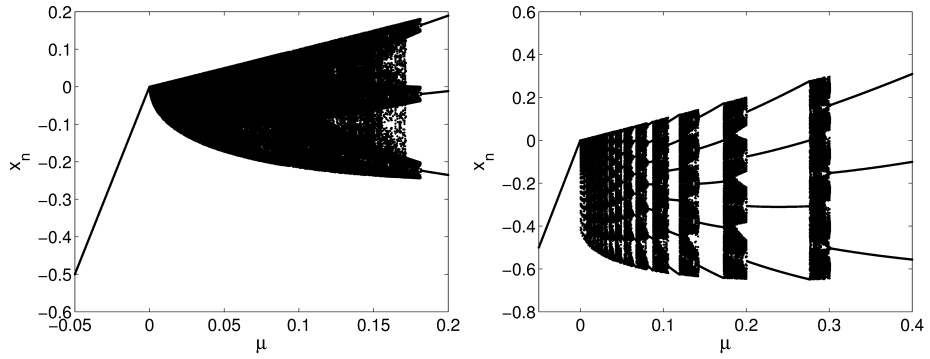

(a) $l = 0$

(b) $l = 0.4$

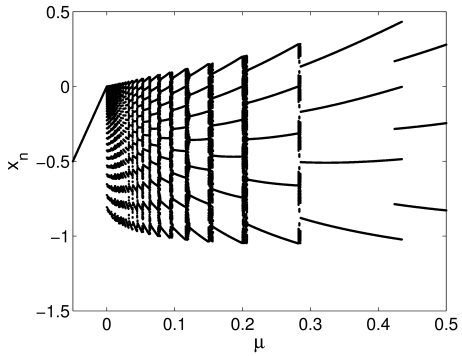

(c) $l = 0.8$

Fig. 3.5: The bifurcation diagrams for the map (2.6) with $\lambda = 0.9$ and $l = \{0, 0.4, 0.8\}$. We see the existence of robust chaos and a period-3 orbit when $l = 0$. In contrast we see very many periodic orbits for larger values of l.

implying that the period-4 orbit exists for $l > 0.08$. Similarly the period-5 orbit exists for $l > 0.19$. Each orbit then has an interval of existence which increases as l increases. We can see from this figure that the regions of existence of the period-3 and period-4 orbits do not intersect if $l = 0.4$, and do intersect if $l = 0.9$.

The difference between the cases of $l = 0$ and $l > 0$ is most apparent in the case of period-N orbits for the case of N large and μ small, and we can summarise this in the following Proposition.

PROPOSITION 3.2. (i) *If $l = 0$ and $\lambda > 2/3$ then for sufficiently large N, no period-N orbits exist.*

(ii) *If $l > 0$ then stable period-N orbits exist over an non-empty interval of values of μ for all $0 < \lambda < 1$ and for all sufficiently large N.*

Proof. The result *(i)* has already been quoted, but for completeness we prove it

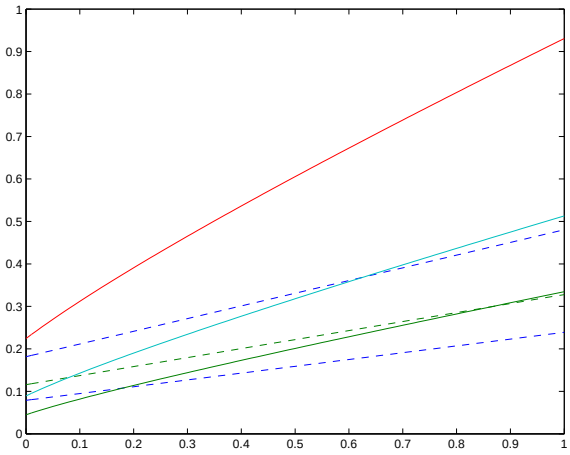

Fig. 3.6: A plot of the period-doubling bifurcation values $\mu_{PD,5} < \mu_{PD,4} < \mu_{PD,3}$ denoted by the dashed lines and the border-collision values $\mu_B C, 5$

¡ $\mu_{BC,4} < \mu_{BC,3}$ as functions 0f l and for $\lambda = 0.9$. A periodic orbit exists if $\mu_{PD,N} < \mu_{BC,N}$. We see how the region of robust chaos for $l = 0$ evolves into a region in which we have a period-adding cascade of maximal orbits.

here. If N is sufficiently large and if $l = 0$ we have asymptotically

$$\mu_{PD,N} \approx \frac{3}{4}(1-\lambda)\lambda^{2N-2} \quad \text{and} \quad \mu_{BC,N} \approx (1-\lambda)^2\lambda^{2N-4}.$$

Thus, $\mu_{PD,N} > \mu_{BC,N}$ if

$$\frac{3}{4}\lambda^2 > (1-\lambda) \quad \text{that is if} \quad \lambda > \frac{2}{3}.$$

Hence no period-N orbit exists in this case.

To prove *(ii)* we note that if $l > 0$ and if N is large then

$$\mu_{PD,N} \approx l\lambda^{N-1}(1-\lambda) \quad \text{and} \quad \mu_{BC,N} \approx l\lambda^{N-2}(1-\lambda).$$

Thus, as $\lambda < 1$ we have

$$\mu_{PD,N} < \mu_{BC,N}$$

and the period-N orbit exists. We note further that the length of intervals of existence Ω_N of the period-N orbits decreases by a factor of λ as N increases by one, and that

$$\mu_{BC,N+1} \approx \mu_{PD,N} < \mu_{BC,N} \approx \mu_{PD,N-1}. \tag{3.1}$$

□

We illustrate the conclusions of this Proposition by plotting in Figure 3.7 the bifurcation diagram for $l = 0.8$ and $\lambda = 0.9$ but this time looking more closely at the high N period-N orbits arising when μ is close to zero. In this figure we can clearly see the existence of these orbits, the geometric scaling of the length of the intervals of existence, and the immediate transition from Ω_{N+1} to Ω_N as a result of (3.1).

4. Conclusions. The introduction of an active impact into the normal impact law for an impact oscillator has led to an interesting map with new dynamics close to a grazing event. In particular, although the map inherits some of the structure of the square-root map, the map has many new periodic orbits. These appear also in the full two-dimensional map describing the more complete dynamics of the active impact problem. Of course this is only the first step in understanding the true dynamics of the pin-ball machine which must also include considerations of the effects of the two-dimensionl motion of the pin-ball and even the effects of human and mechanical interaction. We leave this as a result of further investigation which will of course involve close team work between mathematicians and mechanical engineers.

REFERENCES

[1] C. Budd and F. Dux, *Chattering and related behaviour in impact oscillators*, Philos. Trans. R. Soc. Lond. A, 347 (1994), pp. 365–389.

[2] D. Chillingworth, *Discontinuity geometry for an impact oscillator*, Dyn. Syst., 17 (2002), pp. 389–420.

[3] W. Chin, E. Ott, C. Grebogi, and H. Nusse, *Grazing bifurcations in impact oscillators*, Phys. Rev. E, 50 (1994), pp. 4427–4444.

[4] M. di Bernardo, C. Budd, and A. Champneys, *Normal form maps for grazing bifurcations in n-dimensional piecewise-smooth dynamical systems*, Physica D, 160 (2001), pp. 222–254.

[5] M. di Bernardo, C. Budd, A. Champneys, and P. Kowalczyk, *Piecewise-smooth Dynamical Systems: Theory and Applications*, Springer, 2008.

[6] S. Foale and S. Bishop, *Bifurcations in impact oscillators*, Nonlinear Dynam., 6 (1994), pp. 285–299.

[7] J. Molenaar, J. de Weger, and W. van de Water, *Mappings of grazing-impact oscillators*, Nonlinearity, 14 (2001), pp. 301–321.

[8] A. Nordmark, *Non-periodic motion caused by grazing incidence in impact oscillators*, J. Sound Vibration, 145 (1991), pp. 279–297.

[9] ———, *Universal limit mapping in grazing bifurcations*, Phys. Rev. E, 55 (1997), pp. 266–270.

[10] ———, *Existence of periodic orbits in grazing bifurcations of impacting mechanical oscillators*, Nonlinearity, 14 (2001), pp. 1517–1542.

[11] M. Oestreich, N. Hinrichs, and K. Popp, *Bifurcation and stability analysis for a non-smooth friction oscillator*, Archive of Applied Mechanics, 66 (1996), pp. 301–314.

[12] P. Piiroinen, L. Virgin, and A. Champneys, *Chaos and period-adding; experimental and numerical verification of the grazing bifurcation*, Journal of Nonlinear Science, 14 (2004), pp. 383–404.

[13] S. Shaw and P. Holmes, *A periodically forced piecewise linear oscillator*, Journal of Sound and Vibration, 90 (1983), pp. 129–155.

[14] J. Thompson and R. Ghaffari, *Chaos after period-doubling bifurcations in the resonance of an impact oscillator*, Phys. Lett. A, 91 (1982), pp. 5–8.

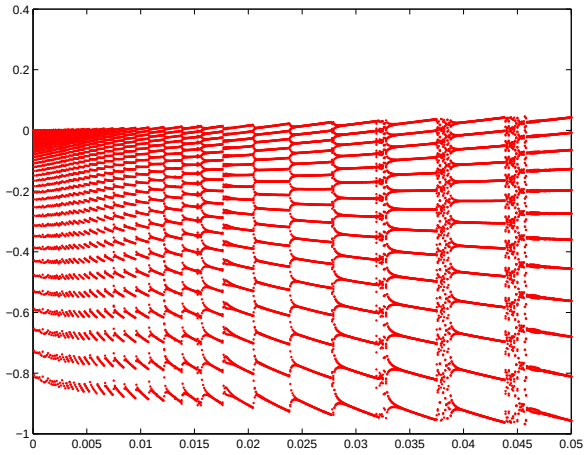

Fig. 3.7: A plot of the bifurcation diagram of the ω-limit set as a function of μ for $l = 0.8$ and $\lambda = 0.9$ showing a close up of the behaviour for values of μ close to zero. Note the existence of the high N period-N orbits, the geometric scaling of the length of the intervals of existence and the immediate transition between the regions of existence implied by (3.1).

[15] G. Whiston, *Global dynamics of a vibro impacting linear oscillator*, Journal of Sound and Vibration, 118 (1987), pp. 395–429.